

Micromixing with In-Flight Charging of Polymer Solutions in a Single Step Enables High-Throughput Production of Micro- and Nanofibers

Luis B. Modesto-López* and Jesús Olmedo-Pradas

Cite This: *ACS Omega* 2022, 7, 12549–12555

Read Online

ACCESS |



Metrics & More

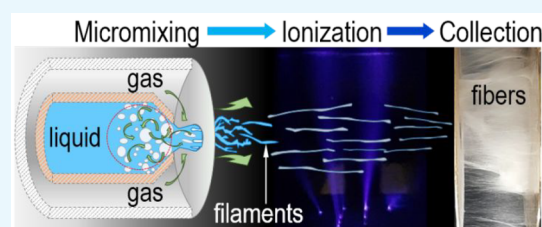


Article Recommendations



Supporting Information

ABSTRACT: Controlled ejection of liquids at capillary scales is a ubiquitous phenomenon associated with significant advances in, for instance, molecular biology or material synthesis. In this work, we introduce a high-throughput approach, which relies on a micromixing mechanism to eject and fragment viscous liquids, for production of microfibers from poly(vinyl alcohol) solutions. First, filaments were generated pneumatically with a so-called flow-blurring atomizer and using liquid flow rates of up to ~ 1 L/min. Subsequently, the filaments were ionized online by corona discharge and consecutively manipulated with an electric field created by disc electrodes. Such charging of the filaments and the effect of the electric field allowed for their ultrafast elongation and diameter reduction from $150 \mu\text{m}$ down to fibers of 500 nm , which after collection exhibited fabric-like texture. The approach presented herein is a general procedure with potential for scalability that, upon proper adaptation, may be extended to various polymeric materials.



INTRODUCTION

Polymer micro- and nanofibers constitute the building blocks of a plethora of structures, and their processing is a field of intense research due to a high demand from emerging technological applications including novel filtration strategies,^{1,2} tissue engineering,³ platforms for wearable textiles,⁴ energy production and storage devices,⁵ and others. The fibers' optimal size, morphology, composition, and three-dimensional arrangement are dictated by the application and depend on the method of preparation. The wide applicability of fibrous structures is due to their mechanical properties, variety of surface functionality, and large surface-area-to-volume ratio.^{6–12}

Typically, microfiber production entails the simultaneous ejection and elongation of a submillimeter-sized jet of a polymer solution.^{13–16} Depending on the physical nature of the process, the continuous jet may give rise to one or multiple filaments,^{14,17–19} which herein are considered to be smaller structures in the liquid state. Further processing leads to reduction of the cross section of the jet or filaments down to a size where solvent rapidly evaporates and the polymer solidifies, thus resulting in microfibers. The entire process usually occurs in a time scale of milliseconds and, in most widespread techniques, is driven by a combination of mechanical and electrical forces.^{20–24} Noticeably, the driving force should be sufficiently strong to overcome capillary forces, such as surface tension, which promote breakup of the jet or filament into droplets. The interplay of forces influencing the fiber formation may be evaluated by the Ohnesorge (Oh)

number, a dimensionless quantity representing the ratio of viscous to inertial forces²⁵

$$\text{Oh} = \mu / \sqrt{\rho_1 R \sigma} \quad (1)$$

where ρ_1 is the density of the liquid; R is a characteristic length scale (typically the radius of the jet or filament); and μ and σ are the solution's viscosity and surface tension, respectively. Longer, straight filaments are produced under conditions such that $\text{Oh} \geq 1$ because of the dominance of viscocapillary forces. Conversely, the dominance of inertia-capillary forces, $\text{Oh} < 1$, may lead to the breakup of the filament into droplets or to the formation of so-called bead-on-a-string (BOAS) structures if the liquid exhibits viscoelasticity.^{7,25–28} Nevertheless, the nanofiber synthesis techniques that are considered to be technologically effective employ an electrical means to provide a driving mechanism for filament elongation and rapid solvent evaporation and operate with relatively low liquid flow rates, from tens of $\mu\text{L}/\text{min}$ to a few mL/min at most, thus resulting in low fiber production rates.^{6,29,30} Additionally, in order to achieve fibers with nanoscale dimensions, the electrical conductivity of the solution should be increased by inclusion of a salt at the expense of reducing the solution's viscosity³¹

Received: October 7, 2021

Accepted: February 28, 2022

Published: April 7, 2022



and adding materials that may subsequently need removal. The technological challenges faced by those approaches were recently highlighted.⁶

Here, we present an alternative method capable of producing microfibers with processing rates of tens of mL/min up to a few L/min (depending on geometrical constraints) and with high potential for scalability. The approach combines filament ejection and in-flight charging, followed by microfiber collection, all in a single step. Indeed, we have termed this polymer processing technology as micromixing with in-flight charging (MIC). The first step, which is filament ejection, is based on the fragmentation of a bulk liquid, due to an energetically efficient micromixing mechanism using a robust flow blurring (FB) atomizer, a device generally employed to produce ultrafine droplets.^{32–36} The atomizer consists of two concentric capillaries in which a gas current radially implodes into the inner tube carrying the liquid, thus triggering the vigorous mixing and causing the disintegration of the liquid bulk into smaller structures. These ejecta may be comprised of either droplets or filaments, depending on the viscous characteristics of the liquid^{32,34,37,38} (see Figure 1a). That is,

RESULTS AND DISCUSSION

In this work, poly(vinyl alcohol) (PVA) solutions were used as test liquids. Figure 1b–d shows frames from ultra-high-speed videos (recorded at one million fps) of as-ejected filaments at varying distance from the FB device outlet (l). The images correspond to filaments of 6 wt % PVA in a mixture of ethanol/water with a mass fraction of water of 0.35 ($\chi_w = 0.35$). Typical values of filament diameter achieved with this method are of the order of 150 μm , which are ejected with mean speeds of approximately 80–100 m/s.^{32,39} Previous analyses have shown that for a range of viscosities and liquid flow rates the mean as-ejected filament diameter, D_f , is determined by the thickness of a liquid boundary layer (δ) that develops in the interior of the atomizer,^{37,40} in the vicinity of its exit orifice of diameter D as depicted in Figure 1. D_f is calculated with a nondimensional relationship (see Figure 8 in Ramos-Escobar et al.³⁷ and analyses therein):

$$D_f^* \sim KQ^{*1/5} \quad (2)$$

where D_f^* and Q^* are nondimensional quantities, filament diameter, and liquid flow rate, respectively, and K is a prefactor of order unity.^{37,40} The derivation of eq 2 was based on Kolmogorov's energy cascade arguments where the dissipation of turbulent energy through viscous mechanisms was taken into account. Thus, instants just after the ejection, the solution's viscosity plays a key role in the filament formation and elongation. Particularly, it was found that in the case of polymer solutions the zero-shear viscosity (μ_0) is critical both in establishing the operation regime for filament formation with micromixing devices and in determining the size of the as-ejected filaments.^{37,38} Polymer solutions with $\mu_0 \geq 10^{-2}$ Pa·s readily form filaments with this technology, provided that the dimensionless quantity $\phi = cM_w/M_e$ is equal to or larger than unity; that is, $\phi \sim 1$ sets the onset for filament formation, where c is the polymer concentration expressed as mass fraction and M_w and M_e are the polymer's molecular weight and entanglement molecular weight, respectively.³⁸ While for cases where $\phi < 1$ ejection of polymer solutions resulted in the formation of droplets,³³ for $\phi > 1$ the as-ejected filaments had lengths of the order of hundreds of micrometers (Figure 2, see inset in red rectangle).

At the typical ejection speeds (~ 80 – 100 m/s^{32,38,39}), however, the residence time, t_R , in an experimental system, such as that depicted in Figures 2 and S1 and with a total length of ~ 0.2 m, would be 2.5 ms, which is relatively short, thus requiring sufficiently high energy, from an external source, to elongate and dry the filaments. To overcome such challenges, the as-ejected filaments were ionized online, which allowed for their further manipulation with electric fields, without addition of salts to increase their electrical conductivity. The ions were produced by a corona discharge device in a so-called needle-to-plate (NtP) configuration and fabricated in-house using 3D printing. Corona discharge is one of the most common techniques for production of ions at atmospheric pressure and has found numerous industrial applications in electrostatic coating and particle collection.^{41–45} In a standard NtP corona ionizer, an electrical breakdown of a gas takes place in the vicinity of the needle's tip, owing to application of a high electrical potential of a few kilovolts. Then, ions of the same polarity as that of the applied voltage travel toward the plate counter electrode, thus creating an ion flux, while those of opposite polarity flow through the

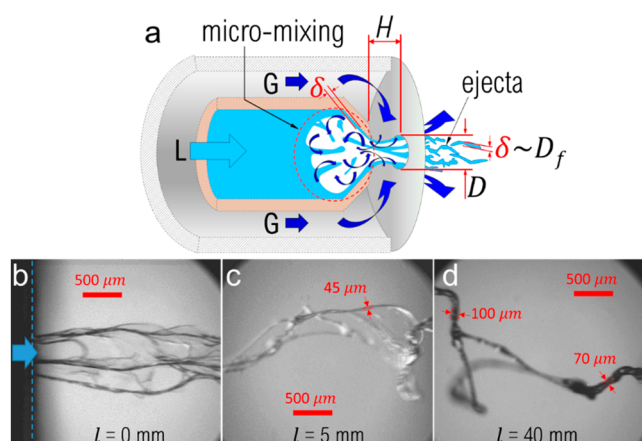


Figure 1. (a) Sketch of cross-sectional view of the FB atomizer; L and G indicate liquid and gas flows, respectively. (b–d) Frames from ultra-high-speed videos (10^6 fps) of ejected filaments from PVA solutions ($M_w = 205\,000$ g/mol, 6 wt % in ethanol/water 65/35 w/w). The frames correspond to different ejection events performed under similar experimental conditions. “ l ” is the distance from the atomizer outlet.

micromixing of low-viscosity Newtonian liquids, such as water, results in ejection of droplets, i.e., a spray. Conversely, micromixing of viscous liquids produces relatively long filaments. In the case of polymer solutions, the filaments are created because the mechanical energy carried by the gas is efficiently transferred into the liquid to create a new surface and then because viscous forces dominate over capillary forces. At this stage, the role of polymer chains is crucial for preventing the breakup of the filaments into droplets and maintaining the one-dimensional shape.

Subsequently, in this MIC approach the polymer filaments were exposed to an ionization zone created by means of corona discharge. Afterward, the as-charged filaments enter an electric field established by a series of circular plates, which serve as collectors, connected to high voltage (see Figure 2). It is within those plates that the filaments rapidly elongate, dry, and form fibers. The entire process, from filament ejection to fibers' formation, takes place online, in a single step.

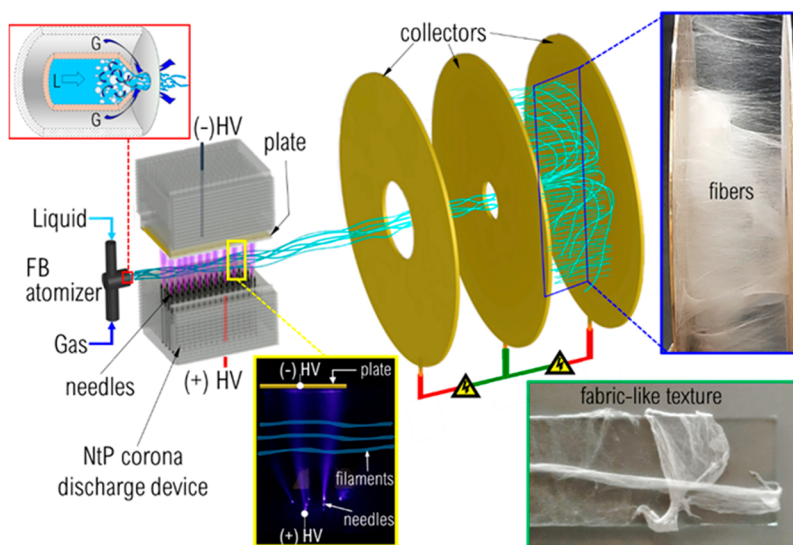


Figure 2. Generation of polymer filaments with the micromixing mechanism using an FB atomizer, followed by in-flight ionization with a corona discharge device and collection using electric fields with disc electrodes. The NtP corona discharge device was 3D printed and consisted of two main components: a plate holder and pin needles holder: (+) HV: +10 kV, (−) HV: −10 kV. The middle collector is electrically grounded, while the other two plates are connected to +10 kV. The collected PVA fiber mats had a fabric-like texture.

Table 1. Mean Filament Diameters from a 6 wt % PVA Solution at $\chi_w = 0.35$

Q_l [mL/min]	μ_0 [Pa·s]	μ [Pa·s]	σ [N/m]	ρ_l [kg/m ³]	ΔP_g [kPa]	Q_g [L/min]	ALR [·] ^a	D_f [μm] ^b
8	25	0.4	0.0324	885.3	178	8	1.38	144
10							1.05	152
16							0.69	165

^aALR: air to liquid mass ratio. Density of air was taken as 1.225 kg/m³. ^b D_f calculated with eq 2, where K takes the value of 0.4, and using the parameters of Table 1; see eqs 4–12 in Ramos-Escobar et al.³⁷

needle (see Figure 2, inset in yellow rectangle). The air breakdown is characterized by giving off ozone odor and by the appearance of a glow at the needle's tip. At sufficiently high electrical potential, the ion flux produces a so-called ionic wind and may be observed by the naked eye as a violet "spray" emitted from the needle. Our NtP device consisted of two main components, which were 3D printed with UV resin, a holder for 64 pin needles and a holder for a metal plate, and typical current values measured across a 40 mm gap (NtP distance) were of the order of 1 μA . The details of the ionizer are depicted in Figure S1. As the filaments passed through the ionizer, they were exposed to a zone of high ion concentration, in-flight, and thus acquired some charge that would play a key role in their elongation. Such elongation due to charging is reminiscent of the jet elongation during electrospinning.^{46,47} Furthermore, the online ionization eliminates the need for increasing the electrical conductivity of the solution and postprocessing steps to remove additives. The charged filaments were then passed through a series of metal disc electrodes where they elongated and formed microfibers in a very short time scale (Figure 2, see inset in blue rectangle). Considering that the t_R of the filaments is approximately 2.5 ms, the filament elongation and drying should have occurred in a much shorter time range. The electric field ultimately provides the driving force acting on the charged filaments, and its role is thus crucial in microfiber formation. Macroscopically, the fibers seemed to be aligned with a direction primarily perpendicular to the discs' main surfaces, although when observed under the electron microscope they had orientations

in various directions, probably because of the inherent randomness of the process and the electrostatic repulsion between themselves. The PVA nonwoven microfibers were removed from the discs and placed on a glass substrate, and they exhibited a delicate fabric-like texture (Figure 2, inset in green rectangle).

This MIC technology was tested using three different liquid flow rates, Q_l , for a constant gas flow rate Q_g as summarized in Table 1. The PVA solutions used herein exhibited a relatively high zero-shear viscosity of 25 Pa·s at a shear rate of 10^{-2} s^{-1} , which decreased down to a nearly Newtonian range (0.4 Pa·s) at about 1 s^{-1} (Figure S2). D_f values of filaments produced with a micromixing device of $D = 100 \mu\text{m}$ and $H = 700 \mu\text{m}$ (see Figure 1) are summarized in Table 1 and were of the order of 150 μm .

Furthermore, the diameter of a viscoelastic filament decreases exponentially according to²⁸

$$D_{f(t)} = D_f \exp\left(-\frac{t}{3\lambda}\right) \quad (3)$$

where $D_{f(t)}$ is the mean diameter of the filaments at time t and λ is the characteristic relaxation time of the fluid. For a PVA of 6 wt % in an ethanol–water mixture, a reasonable estimate for λ would be of the order of 30 ms.⁴⁸ Thus, in the absence of external forces, a filament with an initial diameter of $D_f = 150 \mu\text{m}$ would experience a reduction of only $\sim 3\%$ in $t = t_R = 2.5 \text{ ms}$, that is, $D_f(2.5 \text{ ms}) = 146 \mu\text{m}$. As observed in the SEM images of Figure 3, fibers with diameters at least 3 orders of magnitude smaller than their precursor filaments were

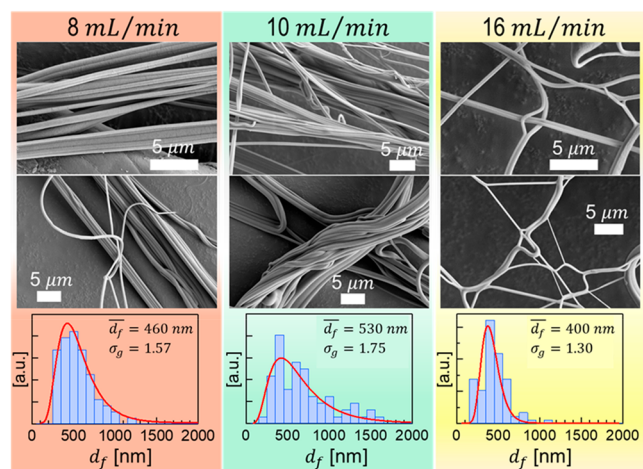


Figure 3. SEM images of PVA fibers produced with FB and corona ionization (see Table 1 for process parameters). Images in a column belong to the same sample. The corresponding fiber size distribution is at the bottom of each column.

obtained, thus evidencing the effect of charging. That is, if only the viscoelastic effect is considered, the expected fiber diameter, d_f would be $146 \mu\text{m}$ which necessarily implies a time much larger than 2.5 ms for the solvent to evaporate and form fibers. Therefore, the rapid transformation from filaments to microfibrils attributed to a significant reduction of the initial filaments' diameter, due to their elongation between the collector electrodes, which is enhanced by the charging with corona ions. The microfibrils' diameters followed a log-normal distribution with geometric mean diameters (\bar{d}_f) in the range 400–530 nm and with geometric mean standard deviations, σ_g , that point to a polydisperse nature. The size of the fibers evidence the effectiveness of the process in reducing the size of as-ejected filaments, without any additives, and using feeding rates with increased industrial relevance compared to other methods.⁶ Note that the distribution of fibers produced with $Q_f = 16 \text{ mL/min}$ shows a tendency toward monodispersity ($\sigma_g < 1.4$) despite being the highest liquid flow rate employed. Under such experimental conditions, one would intuitively expect the formation of thicker fibers. Nevertheless, in calculating the size distribution, only fibers with well-defined boundaries were considered, and irregular BOAS or globular structures produced therein were ignored. In this case, the fibrous structure contained several globular structures (Figure 4a), implying that despite the charging and application of the electric field a fraction of the filaments not only did not elongate (because of high flow rate and short t_R) but also did not breakup and rather formed the irregular structures, most

probably because of the viscoelasticity of the solution. Indeed, some of the micrometer-sized globular structures show relics evidencing filament ejection from their surfaces, thus indicating that at some point the globular structures developed surface instabilities because of their charge.^{49,50} Such instabilities led to the formation of so-called Taylor cones followed by expulsion of mass in the form of a thin jet which quickly dried. Figure 4b shows an SEM image depicting typical fibrous structures produced with the MIC approach, where also randomly oriented straight microfibrils and BOAS of varying sizes (red rectangle and blue oval) are observed. It is noteworthy to mention that when both the ionizer and the HV on the collectors were “off” fibers did not form, and instead the filaments impacted the last collector plate, forming a liquid pool. When the ionizer was “off” and the HV on the collectors was “on”, relatively thick filaments were deposited onto the last collector plate and formed fibers, and also a small fraction of “weak” filaments developed across the plates, that is, oriented perpendicular to the plates' main surface where they dried and formed fibers. Nevertheless, the dense fibrous network as that of Figure 2 was formed only when both the ionizer and the HV on the collectors were “on”, thus evidencing the effect of the corona charging on the fiber formation.

In addition, Figure 4c shows images from an ancillary test with poly(ethylene oxide) (PEO, $M_w = 600\,000 \text{ g/mol}$, 0.8 wt % in ethanol/water 75/25 w/w). In this case, curious structures were obtained, which resemble micro- and nanofibers rolled with “microbandages” that themselves are formed by even smaller, nanometer-sized fibers. For this case, an external heat source was employed, and thus, in addition to the electric field, there may be an effect of much more rapid solvent evaporation. Nevertheless, further studies are needed to elucidate the interplay of mechanisms taking place in fiber formation.

This study introduces an alternative and scalable approach to synthesize polymer micro- and nanofibers with high production rates. The method is based on a high-throughput liquid ejection device that served to fragment PVA and PEO solutions and generate submillimeter-sized filaments, which after suitable ionization are transformed into microfibrils using electric fields. The applicability of this MIC technology may be extended to other viscous materials since the effectivity of the micromixing ejection has been demonstrated for liquids with viscosities in the range 0.001–1 Pa·s.^{34,38,40,51} The rheological properties leading to fragmentation and filament formation with the micromixing mechanism have been assessed for widely used polymers; however, a systematic study is needed to elucidate the interplay of parameters affecting microfiber formation, such as the liquid flow rate or the extent of the ionization. For instance, future studies would point to the use

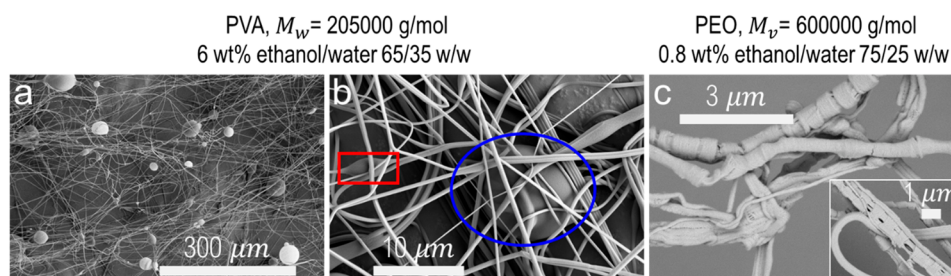


Figure 4. (a) and (b) SEM images of nonwoven PVA fabrics formed by microfibrils. (c) “Microbandage” structures from PEO solutions.

of FB atomizers that operate with liquid flow rates of the order of hundreds of L/min, for which proper corona ionizers should be designed. The capability of synthesizing randomly oriented nonwoven microfiber-based fabrics with high productivity means this MIC technology may be suitable for industrial scalability. The liquid ejection and charging steps presented herein could be of benefit for other material processing technologies.

MATERIALS AND METHODS

Materials. Poly(vinyl alcohol) (PVA, Mowiol 40–88) of average molecular weight of 205 000 g/mol was purchased from Sigma-Aldrich and used as received. PVA was selected as a test polymer due to its high solubility in water and because it is used in high-value-added technological applications, including face masks and electrodes for energy production and storage devices. A mixture of deionized water (Milli-Q) and ethanol was used as the solvent.

Preparation of Solutions. The solution was prepared following the protocol described in our previous publications.^{33,37,38,40} Briefly, a 6 wt % PVA solution in a water/ethanol mixture (water mass fraction, $\chi_w = 0.35$) was prepared by adding a weighted mass of polymer powder to the solvent followed by stirring using a hot plate (Corning PC-420D) until a transparent solution was obtained. The stirring was carried out in a water bath by applying mild heating to facilitate mixing. Other relevant parameters of the polymer solution are surface tension, σ , and density, ρ_v , which in this case are 0.0324 N/m and 885.3 kg/m³, respectively. The solution was allowed to cool to room temperature before liquid ejection experiments.

Viscosity Measurements. To investigate the solution's zero-shear viscosity (μ_0) and to elucidate the shear viscosity over a wide range of shear rate, the solution was characterized using a TA Instruments rheometer (Discovery HR-3) with cone–plate configuration with a gap of 52 μm . The cone angle and the plate diameter were 2.009° and 60 mm, respectively. In addition, the instrument is equipped with a Peltier plate to allow control of temperature. μ_0 was taken as the viscosity corresponding to the lowest shear rate. The measurement was performed at room temperature and ambient relative humidity (in the range of 50–60%). The results are depicted in Figure S2.

Ionizer. The ionizer was constructed based on an in-house design using 3D printing (UV resin). It consists of two main components (see Figure S1), a needle holder and a plate holder, both separated by a gap, h , of ~ 40 mm in which the ionization zone is created. The needle holder had a quadrangular shape with a base of 40 mm \times 55 mm and a height of 33 mm. This holder had 1 mm circular holes perforated thru to allow for insertion of 64 pin needles of 34 mm of nominal length. A channel in the interior of the holder allowed for connecting all the needles, by means of a copper wire, to the same positive potential through a high-voltage (HV) supply. The plate holder had similar dimensions as that of the needles, but it had a slot to slide in a brass plate that served as a negative electrode. A copper cable was welded to the plate to connect it to a high voltage power supply. The potentials applied to the needles and to the plate were +10 kV and –10 kV, respectively, and typical current values measured across the 40 mm gap, for 64 needles, were of the order of 1 μA . Under such conditions, a characteristic corona glow could be observed by the naked eye, and white noise was also heard.

Atomization and Collection. Figure S3 depicts the overall experimental setup consisting of a liquid ejection device, the corona ionizer, and a collection system. The liquid ejection and filament generation procedure is similar to that reported in our previous work using an FB device (Ingeniatrias Tecnológicas, Seville, Spain) with nominal orifice diameter $D = 700$ μm and gap $H = 100$ μm (see Figure 1a).^{33,37,38,40} The device has two inlets, for liquid and gas, which in this case is air. The gas overpressure (ΔP_g), of the order of 200 kPa, is measured with a digital manometer to deliver a gas flow rate, Q_g , of approximately 8 mL/min, as recorded by a digital flow meter. The polymer solution is supplied pneumatically by feeding pressurized air into a liquid container to result in liquid flow rates, Q_l , in the range of 8–16 mL/min. Q_l was controlled by adjusting the gas overpressure in the container, ΔP_l . For more details of the internal geometry of the FB atomizer and its functioning, the interested reader may refer to refs 34, 37, 38, and 40. Notice that both liquid filaments and air come out the atomizer, and this air current acts as sheath air flow.

The as-generated filaments were passed through the field ionization zone, described previously, and subsequently directed toward the collection system, which consisted of three brass discs with diameter of 250 mm. The discs, centered and aligned along the filament ejection axis, were spaced by 50 mm. The first and second discs had circular perforations of 50 mm and 35 mm in diameter, respectively, to allow for the sheath air and the filaments to pass through. In addition, the first and third discs were maintained at a high potential of +10 kV, while the central disc was electrically grounded. The established electric field served to decelerate the charged filaments and simultaneously stretch them to reduce their size and form fibers in a relatively short period of time.

In terms of system operation, first, the ionizer is activated by applying the high and negative potentials, and subsequently the electric field in the collector is established. Then, the FB atomizer is operated by feeding air, and once the flow is stabilized, the liquid is supplied pneumatically. All experiments were conducted under atmospheric conditions at an average ambient temperature and relative humidity of 25 °C and 45%, respectively.

ASSOCIATED CONTENT

Supporting Information

The Supporting Information is available free of charge at <https://pubs.acs.org/doi/10.1021/acsomega.1c05589>.

Diagrams of ionizer and of detailed experimental setup.
Viscosity data of PVA solutions used in experiments.
SEM image of fibers obtained with ionizer “off” (PDF)

AUTHOR INFORMATION

Corresponding Author

Luis B. Modesto-López – Department of Aerospace Engineering and Fluid Mechanics, ETSI, Universidad de Sevilla, 41092 Sevilla, Spain; orcid.org/0000-0002-9493-8846; Email: lmodesto@us.es

Author

Jesús Olmedo-Pradas – Department of Aerospace Engineering and Fluid Mechanics, ETSI, Universidad de Sevilla, 41092 Sevilla, Spain

Complete contact information is available at: <https://pubs.acs.org/10.1021/acsomega.1c05589>

Author Contributions

The manuscript was written through contributions of all authors. All authors have given approval to the final version of the manuscript.

Notes

The authors declare no competing financial interest.

ACKNOWLEDGMENTS

L.B.M.L. acknowledges financial support from Consejería de Economía, Conocimiento, Empresas y Universidades of Junta de Andalucía (Spain), through a PAIDI 2020 grant (number P18-FR-3623) and a FEDER grant (number US-1380775).

REFERENCES

- (1) Ullah, S.; Ullah, A.; Lee, J.; Jeong, Y.; Hashmi, M.; Zhu, C.; Joo, K. I.; Cha, H. J.; Kim, I. S. Reusability Comparison of Melt-Blown vs Nanofiber Face Mask Filters for Use in the Coronavirus Pandemic. *ACS Appl. Nano Mater.* **2020**, *3* (7), 7231–7241.
- (2) Lu, T.; Cui, J.; Qu, Q.; Wang, Y.; Zhang, J.; Xiong, R.; Ma, W.; Huang, C. Multistructured Electrospun Nanofibers for Air Filtration: A Review. *ACS Appl. Mater. Interfaces* **2021**, *13* (20), 23293–23313.
- (3) Rahmati, M.; Mills, D. K.; Urbanska, A. M.; Saeb, M. R.; Venugopal, J. R.; Ramakrishna, S.; Mozafari, M. Electrospinning for Tissue Engineering Applications. *Prog. Mater. Sci.* **2021**, *117*, 100721.
- (4) Chen, J.; Huang, Y.; Zhang, N.; Zou, H.; Liu, R.; Tao, C.; Fan, X.; Wang, Z. L. Micro-Cable Structured Textile for Simultaneously Harvesting Solar and Mechanical Energy. *Nat. Energy* **2016**, *1* (10), 1–8.
- (5) Wang, X.; Liu, B.; Liu, R.; Wang, Q.; Hou, X.; Chen, D.; Wang, R.; Shen, G. Fiber-Based Flexible All-Solid-State Asymmetric Supercapacitors for Integrated Photodetecting System. *Angew. Chemie - Int. Ed.* **2014**, *53* (7), 1849–1853.
- (6) Müller, F.; Jokisch, S.; Bargel, H.; Scheibel, T. Centrifugal Electrospinning Enables the Production of Meshes of Ultrathin Polymer Fibers. *ACS Appl. Polym. Mater.* **2020**, *2* (11), 4360–4367.
- (7) Ma, M.; Mao, Y.; Gupta, M.; Gleason, K. K.; Rutledge, G. C. Superhydrophobic Fabrics Produced by Electrospinning and Chemical Vapor Deposition. *Macromolecules* **2005**, *38* (23), 9742–9748.
- (8) Cooper, J. A.; Lu, H. H.; Ko, F. K.; Freeman, J. W.; Laurencin, C. T. Fiber-Based Tissue-Engineered Scaffold for Ligament Replacement: Design Considerations and in Vitro Evaluation. *Biomaterials* **2005**, *26* (13), 1523–1532.
- (9) Tang, C.-S.; Shi, B.; Zhao, L.-Z. Interfacial Shear Strength of Fiber Reinforced Soil. *Geotext. Geomembranes* **2010**, *28* (1), 54–62.
- (10) Zheng, Y.; Bai, H.; Huang, Z.; Tian, X.; Nie, F.-Q.; Zhao, Y.; Zhai, J.; Jiang, L. Directional Water Collection on Wetted Spider Silk. *Nature* **2010**, *463* (7281), 640–643.
- (11) Zeng, W.; Shu, L.; Li, Q.; Chen, S.; Wang, F.; Tao, X.-M. Fiber-Based Wearable Electronics: A Review of Materials, Fabrication, Devices, and Applications. *Adv. Mater.* **2014**, *26* (31), 5310–5336.
- (12) Fratzl, P.; Weinkamer, R. Nature's Hierarchical Materials. *Prog. Mater. Sci.* **2007**, *52* (8), 1263–1334.
- (13) Gupta, D.; Jassal, M.; Agrawal, A. K. Electrospinning of Poly(Vinyl Alcohol)-Based Boger Fluids To Understand the Role of Elasticity on Morphology of Nanofibers. *Ind. Eng. Chem. Res.* **2015**, *54* (5), 1547–1554.
- (14) Xue, J.; Wu, T.; Dai, Y.; Xia, Y. Electrospinning and Electrospun Nanofibers: Methods, Materials, and Applications. *Chem. Rev.* **2019**, *119* (8), 5298–5415.
- (15) Vasireddi, R.; Kruse, J.; Vakili, M.; Kulkarni, S.; Keller, T. F.; Monteiro, D. C. F.; Trebbin, M. Solution Blow Spinning of Polymer/Nanocomposite Micro-/Nanofibers with Tunable Diameters and Morphologies Using a Gas Dynamic Virtual Nozzle. *Sci. Rep.* **2019**, DOI: 10.1038/s41598-019-50477-6.
- (16) Dadol, G. C.; Kilic, A.; Tijjing, L. D.; Lim, K. J. A.; Cabatingan, L. K.; Tan, N. P. B.; Stojanovska, E.; Polat, Y. Solution Blow Spinning (SBS) and SBS-Spun Nanofibers: Materials, Methods, and Applications. *Mater. Today Commun.* **2020**, *25*, 101656.
- (17) Hoath, S. D.; Jung, S.; Hutchings, I. M. A Simple Criterion for Filament Break-up in Drop-on-Demand Inkjet Printing. *Phys. Fluids* **2013**, *25* (2), 021701.
- (18) Yu, L. F.; Zuo, Z. G.; Li, L.; Liu, S. H.; Zhao, S. T. EXPERIMENTAL BREAKUP CHARACTERISTICS OF ROUND LIQUID JETS OF A DILUTE POLYMER SOLUTION INTO QUIESCENT AIR. *J. Appl. Mech. Technol. Phys.* **2020**, *61* (4), 676–684.
- (19) Aliseda, A.; Hopfinger, E. J.; Lasheras, J. C.; Kremer, D. M.; Berchielli, A.; Connolly, E. K. Atomization of Viscous and Non-Newtonian Liquids by a Coaxial, High-Speed Gas Jet. Experiments and Droplet Size Modeling. *Int. J. Multiph. Flow* **2008**, *34*, 161–175.
- (20) Si, T.; Yin, C.; Gao, P.; Li, G.; Ding, H.; He, X.; Xie, B.; Xu, R. X. Steady Cone-Jet Mode in Compound-Fluidic Electro-Flow Focusing for Fabricating Multicompartment Microcapsules. *Appl. Phys. Lett.* **2016**, *108* (2), 021601.
- (21) Acero, A. J.; Rebollo-Muñoz, N.; Montanero, J. M.; Gañán-Calvo, A. M.; Vega, E. J. A New Flow Focusing Technique to Produce Very Thin Jets. *J. Micromechanics Microengineering* **2013**, *23* (6), 065009.
- (22) Ponce-Torres, A.; Ortega, E.; Rubio, M.; Rubio, A.; Vega, E. J.; Montanero, J. M. Gaseous Flow Focusing for Spinning Micro and Nanofibers. *Polymer (Guildf)*. **2019**, *178*, 121623.
- (23) Daristotle, J. L.; Behrens, A. M.; Sandler, A. D.; Kofinas, P. A Review of the Fundamental Principles and Applications of Solution Blow Spinning. *ACS Appl. Mater. Interfaces* **2016**, *8*, 34951–34963.
- (24) Paruchuri, S.; Brenner, M. P. Splitting of a Liquid Jet. *Phys. Rev. Lett.* **2007**, *98* (13), 134502.
- (25) Bhat, P. P.; Appathurai, S.; Harris, M. T.; Pasquali, M.; McKinley, G. H.; Basaran, O. A. Formation of Beads-on-a-String Structures during Break-up of Viscoelastic Filaments. *Nat. Phys.* **2010**, *6* (8), 625–631.
- (26) Yang, Q.; Li, Z.; Hong, Y.; Zhao, Y.; Qiu, S.; Wang, C.; Wei, Y. Influence of Solvents on the Formation of Ultrathin Uniform Poly(Vinyl Pyrrolidone) Nanofibers with Electrospinning. *J. Polym. Sci., Part B: Polym. Phys.* **2004**, *42* (20), 3721–3726.
- (27) Clasen, C.; Eggers, J.; Fontelos, M. A.; Li, J.; McKinley, G. H. The Beads-on-String Structure of Viscoelastic Threads. *J. Fluid Mech.* **2006**, *556*, 283.
- (28) Tirel, C.; Renoult, M.-C.; Dumouchel, C.; Lisiecki, D.; Crumeyrolle, O.; Mutabazi, I. Multi-Scale Analysis of a Viscoelastic Liquid Jet. *J. Nonnewton. Fluid Mech.* **2017**, *245*, 1–10.
- (29) Helgeson, M. E.; Grammatikos, K. N.; Deitzel, J. M.; Wagner, N. J. Theory and Kinematic Measurements of the Mechanics of Stable Electrospun Polymer Jets. *Polymer (Guildf)*. **2008**, *49* (12), 2924–2936.
- (30) Rwei, S.-P.; Huang, C.-C. Electrospinning PVA Solution-Rheology and Morphology Analyses. *Fibers Polym.* **2012**, *13* (1), 44–50.
- (31) Modesto-López, L. B.; Chimentão, R. J.; Álvarez, M. G.; Rosell-Llompart, J.; Medina, F.; Llorca, J. Direct Growth of Hydrotalcite Nanolayers on Carbon Fibers by Electrospinning. *Appl. Clay Sci.* **2014**, *101*, 461–467.
- (32) Modesto-López, L. B.; Gañán-Calvo, A. M. Visualization and Size-Measurement of Droplets Generated by Flow Blurring® in a High-Pressure Environment. *Aerosol Sci. Technol.* **2018**, *52* (2), 198–208.
- (33) Hermosín-Reyes, M.; Gañán-Calvo, A. M.; Modesto-López, L. B. Flow Blurring Atomization of Poly(Ethylene Oxide) Solutions below the Coil Overlap Concentration. *J. Aerosol Sci.* **2019**, *137*, 105429.
- (34) Gañán-Calvo, A. M. Enhanced Liquid Atomization: From Flow-Focusing to Flow-Blurring. *Appl. Phys. Lett.* **2005**, *86* (21), 214101.
- (35) Serrano, J.; Jiménez-Espadafor, F. J.; Lora, A.; Modesto-López, L.; Gañán-Calvo, A.; López-Serrano, J. Experimental Analysis of NOx

Reduction through Water Addition and Comparison with Exhaust Gas Recycling. *Energy* **2019**, *168*, 737–752.

(36) Matusiewicz, H.; Slachcinski, M.; Almagro, B.; Canals, A. Evaluation of Various Types of Micronebulizers and Spray Chamber Configurations for Microsamples Analysis by Microwave Induced Plasma Optical Emission Spectrometry. *Chem. Analityczna* **2009**, *54* (6, Sp. Iss. SI), 1219–1244.

(37) Ramos-Escobar, A.; Uceda-Gallegos, R.; Modesto-López, L.; Gañán-Calvo, A. Dynamics of Formation of Poly(Vinyl Alcohol) Filaments with an Energetically Efficient Micro-Mixing Mechanism. *Phys. Fluids* **2020**, *32* (12), 122101.

(38) Modesto-López, L. B.; Pérez-Arjona, A.; Gañán-Calvo, A. M. Flow Blurring-Enabled Production of Polymer Filaments from Poly(Ethylene Oxide) Solutions. *ACS Omega* **2019**, *4* (2), 2693–2701.

(39) Simmons, B. M.; Agrawal, A. K. SPRAY CHARACTERISTICS OF A FLOW-BLURRING ATOMIZER. *At. Sprays* **2010**, *20* (9), 821–835.

(40) Marín-Brenes, F.; Olmedo-Pradas, J.; Gañán-Calvo, A. M.; Modesto-López, L. On the Ejection of Filaments of Polymer Solutions Triggered by a Micrometer-Scale Mixing Mechanism. *Materials (Basel)* **2021**, *14* (12), 3399.

(41) Bruggeman, P. J.; Iza, F.; Brandenburg, R. Foundations of Atmospheric Pressure Non-Equilibrium Plasmas. *Plasma Sources Sci. Technol.* **2017**, *26* (12), 123002.

(42) Chang, J.-S.; Lawless, P. A.; Yamamoto, T. Corona Discharge Processes. *IEEE Trans. Plasma Sci.* **1991**, *19* (6), 1152–1166.

(43) Levitin, G.; Reinhardt, K.; Hess, D. W. Plasma Cleaning for Electronic, Photonic, Biological, and Archeological Applications. In *Developments in Surface Contamination and Cleaning*; Elsevier, 2013; pp 55–121. DOI: 10.1016/B978-1-4377-7881-6.00002-8.

(44) Pérez Hortal, A. A.; García, S. E.; Caranti, G. M. Droplet Charging by High Voltage Discharges and Its Influence on Precipitation Enhancement. *Atmos. Res.* **2012**, *108*, 115–121.

(45) Kulkarni, P.; Namiki, N.; Otani, Y.; Biswas, P. Charging of Particles in Unipolar Coronas Irradiated by In-Situ Soft X-Rays: Enhancement of Capture Efficiency of Ultrafine Particles. *J. Aerosol Sci.* **2002**, *33* (9), 1279–1296.

(46) Reneker, D. H.; Yarin, A. L.; Zussman, E.; Xu, H. Electrospinning of Nanofibers from Polymer Solutions and Melts. *Advances in Applied Mechanics* **2007**, *41*, 43–346.

(47) Ding, C.; Fang, H.; Duan, G.; Zou, Y.; Chen, S.; Hou, H. Investigating the Draw Ratio and Velocity of an Electrically Charged Liquid Jet during Electrospinning. *RSC Adv.* **2019**, *9* (24), 13608–13613.

(48) Theron, S. A.; Zussman, E.; Yarin, A. L. Experimental Investigation of the Governing Parameters in the Electrospinning of Polymer Solutions. *Polymer (Guildf)*. **2004**, *45* (6), 2017–2030.

(49) Mohamed, A. S.; Lopez-Herrera, J. M.; Herrada, M. A.; Modesto-Lopez, L. B.; Gañán-Calvo, A. M. Effect of a Surrounding Liquid Environment on the Electrical Disruption of Pendant Droplets. *Langmuir* **2016**, *32* (27), 6815–6824.

(50) Wang, Q.; Ma, M.; Siegel, M. Deformation and Stability of a Viscous Electrolyte Drop in a Uniform Electric Field. *Phys. Rev. Fluids* **2019**, DOI: 10.1103/PhysRevFluids.4.053702.

(51) Simmons, B. M.; Agrawal, A. K. Flow Blurring Atomization for Low-Emission Combustion of Liquid Biofuels. *Combust. Sci. Technol.* **2012**, *184* (5), 660–675.